Applied Catalysis B: Environmental 95 (2010) 414–422

Contents lists available at ScienceDirect

Applied Catalysis B: Environmental

journal homepage: www.elsevier.com/locate/apcatb

Photocatalytic degradation of bisphenol-A by nitrogen-doped TiO_2 hollow sphere in a vis-LED photoreactor

Dewi Puspitaningrum Subagio [a], Madhavi Srinivasan [c,*], Melvin Lim [a,b], Teik-Thye Lim [a,b,**]

[a] School of Civil and Environmental Engineering, Nanyang Technological University, Block N1, 50 Nanyang Avenue, Singapore 639798, Singapore
[b] Singapore Membrane Technology Centre, Nanyang Technological University, Nanyang Avenue, Singapore 639798, Singapore
[c] School of Materials Science and Engineering, Nanyang Technological University, Block N4.1, Nanyang Avenue, Singapore 639798, Singapore

ARTICLE INFO

Article history:
Received 9 November 2009
Received in revised form 31 December 2009
Accepted 20 January 2010
Available online 25 January 2010

Keywords:
Nitrogen doping
Hollow spheres
Bisphenol-A
Photocatalytic degradation
Titania

ABSTRACT

Photocatalytic degradation and mineralization of bisphenol-A (BPA) by a novel photocatalyst, nitrogen-doped TiO_2 hollow sphere (NhT), under blue, green and yellow lights emitted by light emitting diodes (LEDs) were investigated. The photocatalyst was synthesized through polystyrene spheres templating and treatment with ammonia to extend its light absorption properties to 550 nm (E_g = 2.26 eV) and meanwhile possess high porosity and specific surface area. Nitrogen incorporation was confirmed through XPS analysis indicating the presence of O–Ti–N or Ti–O–N linkages in the photocatalyst material. The NhT exhibited significant increase of BPA degradation and mineralization under blue, green and yellow lights as compared to the undoped TiO_2 hollow sphere, powder TiO_2, and Hombikat UV100. The photocatalytic degradation of BPA increased with pH, and the rate was the highest even at pH > pKa1 of BPA (i.e., pH 9.6). At circumneutral pH, 90% of BPA was degraded in 2 h under irradiation of blue light with NhT, while TOC removal was 66% after 6 h of irradiation. The main aromatic intermediates formed were identified with GC/MS and LC/MS/MS as 4-hydroxyacetophenone, 4-isopropylphenol, 4-isopropenylphenol and isopropanolphenol. The pathways for BPA degradation under visible light appear to agree with those with UV/TiO_2.

1. Introduction

Bisphenol-A (BPA), a known endocrine disrupting chemical (EDC) and highly toxic compound for aquatic organisms [1], has been widely used for the production of polycarbonate plastics and epoxy resins [2,3] which have a wide range of applications. It is found in various consumer products including baby bottles, food and drink packaging materials, dental sealants, eyeglass lenses, household appliances, electrical equipment, consumer electronics, etc. BPA is recalcitrant and frequently found along with other EDCs in urban wastewaters and treated effluents [4], and is also ubiquitous in surface waters [5,6]. Due to its endocrine disrupting effects, there has been increasing concerns about BPA present in the aquatic and terrestrial environments, and its potential adverse impacts on ecological and public health.

To control BPA release into the environment, there is an increasing interest in developing effective treatment technologies for complete removal of BPA in the recent years. These include adsorption with activated carbon, enhanced biodegradation, thermal destruction and advanced oxidation processes. However, these methods suffer drawbacks such as simply transferring the pollutant from one phase to another without destruction (e.g., adsorption), requiring large energy input (e.g., thermal destruction and ozonation), slow process (e.g., biological treatment), or consuming chemicals (e.g., Fenton/photo-Fenton processes). Heterogeneous photocatalysis for BPA degradation with UV-irradiated titania (TiO_2) has been reported recently [7–16], and it appears to be a potentially cost-effective and environmentally-sustainable treatment alternative. The neat (unmodified) TiO_2 presents high photoactivity even without chemical additives, and is relatively inexpensive, chemically and biologically stable, and of low toxicity, making it the most suitable semiconductor photocatalyst for application in water treatment and reclamation. However, to date, commercial-scale TiO_2 application in water treatment is still limited. One of the reasons for this hindrance is its large bandgap energy (E_g) that requires UV for its photo-excitation and production of powerful hydroxyl radicals (•OH). To enable photo-excitation of TiO_2 with sunlight, there have been numerous attempts to dope TiO_2 with various anions [17], of which nitrogen appears to be the most promising dopant on the basis of spin-restricted local density approximation (LDA) calculations. Based on

* Corresponding author. Tel.: +65 6790 4606; fax: +65 6790 9081.
** Corresponding author at: School of Civil and Environmental Engineering, Nanyang Technological University, Block N1, 50 Nanyang Avenue, Singapore 639798, Singapore. Tel.: +65 6790 6933; fax: +65 6791 0676.
E-mail addresses: madhavi@ntu.edu.sg (M. Srinivasan), cttlim@ntu.edu.sg (T.-T. Lim).

0926-3373/$ – see front matter © 2010 Elsevier B.V. All rights reserved.
doi:10.1016/j.apcatb.2010.01.021

this modeling, N2p states could contribute to bandgap narrowing by mixing with O2p states in the valence band, allowing e^-/h^+ generation under visible light.

Heterogeneous photocatalysis is a surface-mediated advanced oxidation process. Enhanced mass transfer of target pollutants to the surface of photocatalyst and increased surface exposure to photons will increase its photonic efficiency or quantum yield. The hollow sphere structure is thus garnering increasing interest attributed to its high surface area, high porosity and low bulk density. Its increased surface area associated with hollow structure allowing better pollutant access to both exterior and interior photocatalyst surfaces, while its low bulk density enables homogeneous dispersion throughout the photoreactor volume. The TiO_2 hollow sphere can be synthesized by hydrolyzing Ti precursor in the presence of spherical carbonaceous templates [18–23]. After calcinations, the template is removed resulting in hollow spherical morphology with TiO_2 shell.

Rapid advancement of light emitting diodes (LEDs) development has opened the possibility of employing LED as an alternative artificial light source for photoreactors in the absence of solar irradiation. LEDs are known for its long lifetime and energy efficiency. Its smaller size and robustness allow greater flexibility in its array configuration and applications. Its materials can be almost completely recycled at the end of use.

In this study, we report photocatalytic degradation and mineralization of BPA in a batch photoreactor illuminated with vis-LEDs. The novel photocatalyst developed was nitrogen-doped TiO_2 hollow sphere (NhT) synthesized through polystyrene (PS) spheres templating. To evaluate the action spectrum of the photocatalyst and its potential use for solar photocatalysis, different types of LED were used to produce visible lights of varying monochromatic wavelengths and the resulting BPA photocatalysis was compared. The effects of pH on BPA photocatalytic degradation and mineralization were also investigated. To establish the possible BPA photocatalytic degradation pathway under the visible light irradiation, the intermediates formed were also analyzed.

2. Experimental methods

2.1. Synthesis of polystyrene spheres

Monodispersed polystyrene (PS) spheres were synthesized via emulsion–polymerization using styrene (98%, Merck), potassium persulfate (98%, Scharlau), and sodium dodecyl sulfate (96%, Fluka) as the monomer, initiator, and surfactant, respectively. Prior to use, styrene was treated with 0.1 M solution of sodium hydroxide, and rinsed thoroughly with deionized water (Millipore, 18.2 MΩ cm) several times to remove the polymerization inhibitor. Sodium dodecyl sulfate (0.035 M) and potassium persulfate (0.04 M) were dissolved in water in a three-neck flask with stirring. Styrene (25 mL) was then introduced in the flask under both nitrogen bubbling and rapid stirring at 70 °C. The PS spheres, formed after 4 h, were collected by centrifugation and washed several times with water. Finally, a stock suspension of PS spheres was prepared by dispersing in absolute ethanol (Merck).

2.2. Synthesis of photocatalysts

Firstly, titania sol was prepared at room temperature by hydrolyzing titanium isopropoxide (TTIP, Merck) in absolute ethanol (Merck) under vigorous stirring. A stock suspension of PS spheres (20 mL) was introduced under stirring into the titania sol and left to stir for 30 min. This was followed by a static-aging process of 7 days. To prepare N-doped TiO_2 hollow spheres (NhT), ammonium hydroxide (25%, Merck) (added to a N:Ti molar ratio of 1:5) and 0.5 mL of HNO_3 (70%, Labscan) were added into the aged mixture and homogenized by orbital shaking (150 rpm) at room temperature for 2 days. The solid product was collected using centrifugation (8000 rpm, 10 min) and washed with water several times before drying in an oven at 80 °C for 12 h. To determine the appropriate calcination temperature for the dried sample, thermogravimetric analysis was first carried out to investigate decomposition temperature of PS templates. The result (Fig. 1) showed the first weight loss of ca. 10% below 300 °C indicating removal of adsorbed water on the coated spheres, and the subsequent weight losses of ca. 42% (300–460 °C) corresponding to PS templates decomposition. At temperature 500 °C or above, stable weight of sample was observed indicating that PS templates can be completely removed at 500 °C. Therefore, the dried sample of coated PS spheres was calcined at 500 °C for 2 h (ramped up at 5 °C/min) to remove the PS cores. For comparison, pure TiO_2 hollow sphere (hT) and TiO_2 powder (PT) were also prepared by the same procedure without the addition of ammonium hydroxide and/or PS template.

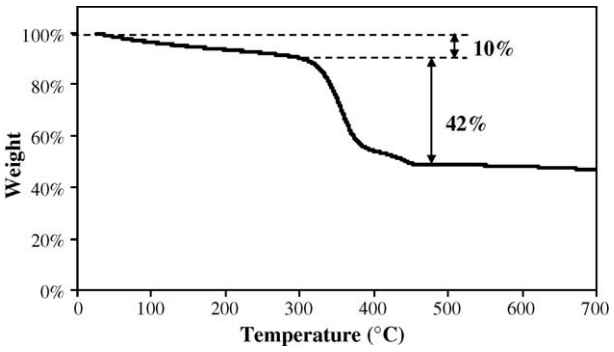

Fig. 1. Thermogravimetric analysis curve of coated PS spheres.

2.3. Photocatalysts characterization

Scanning electron micrographs were obtained using a JEOL 6340F field-emission scanning electron microscope with an accelerating voltage of 5 keV. Samples were coated with platinum using auto fine coater (JEOL JFC-1600). Transmission electron micrographs were obtained using a JEOL 2100F transmission electron microscope working at 200 keV. Porosimetric studies were carried out with a Quantachrome Autosorb I, with samples degassed at 200 °C (16 h) prior to analyses. X-ray diffraction (XRD) patterns were obtained using a Bruker D8 ADVANCE X-ray Diffractometer with CuK_α radiation using step intervals of 0.02° (2θ) at a scan rate of 0.8° (2θ)/min. X-ray photoelectron spectroscopy was carried out with a Kratos Axis XPS using a monochromatized Al Kα X-ray source (1486.71 eV), and charge-referenced using adventitious carbon at 284.8 eV. Absorbance spectra of the photocatalysts were measured using a Perkin Elmer Lambda 35 UV-Visible Spectrophotometer with a scan rate of 120 nm/min. The zeta potential values were obtained using a Malvern nano-zs zetasizer in suspension with photocatalyst concentration of 0.5 g/L. The pH variation was obtained through addition of 0.05 M HCl or 0.05 M NaOH solution.

2.4. LED photoreactor setup

The schematic diagram of the LED photoreactor is depicted in Fig. 2. It comprised a 500 mL borosilicate glass reactor with 80 mm diameter and 110 mm height. The reactor was wrapped with a 2-m long LED flexible strip (SMD 5050, 15 W) comprising 60 LED units (beam angle 120°). The LED strip is 10 mm wide and 2 mm thick.

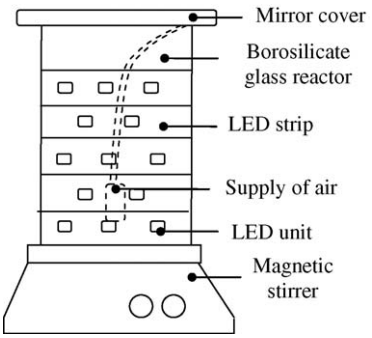

Fig. 2. Schematic diagram of photoreactor used for photodegradation of bisphenol-A with LED strip as excitation light source.

Three different LED strips were used in this study, emitting blue light (main emission wavelength $\lambda = 465$ nm), green light ($\lambda = 523$ nm) and yellow light ($\lambda = 589$ nm), respectively. A cooling jacket was draped around the LEDs-wrapped-reactor to maintain photoreactor temperature at 30 ± 5 °C throughout the experiment run. A mirror cover was used to minimize penetration of light from surrounding and minimize water evaporation.

2.5. Photocatalytic testing

The photocatalytic degradation of BPA was systematically evaluated with the three types of synthesized photocatalysts, while comparison studies with Hombikat UV100 (Sigma–Aldrich; BET surface area > 250 m^2/g and primary crystallite size < 10 nm [24]) were also performed as necessary. Prior to the commencement of each photocatalytic experiment, 400 mL suspension containing 0.2 g of a photocatalyst (dosage = 0.5 g/L) and BPA of 5.0 mg/L was prepared and stirred in the photoreactor in dark for 1 h to establish an adsorption equilibrium of BPA with the photocatalyst. It was observed that at concentration of 5.0 mg/L, the extent of BPA adsorption by various photocatalysts in dark was insignificant. Therefore, this would minimize the complexity in the subsequent analysis of the photocatalytic degradation kinetics which has been often found dependent on the initial concentration of the substrate [9,14].

After commencement of the photocatalytic experiment, sample aliquots were collected at appropriate time intervals and filtered using cellulose acetate syringe membrane filters (Iwaki, 0.45 μm) which showed negligible BPA adsorption compared to other filter types. Photocatalytic degradation of BPA using various photocatalysts was studied under different LED lights (blue, green and yellow). The effect of initial pH was also investigated through pH adjustments with 1 M HCl and 1 M NaOH solutions. A control experiment was carried out at natural pH (6.0 ± 0.2) with 1.25 mM NaCl as the background electrolyte to detect possible effect on the observed BPA photocatalytic degradation rate that could be rather due to Cl^- in the solution. It was observed that the pH values of the solutions remained rather stable throughout the experiment, with typical variation of <0.5 unit. The experiments with synthesized photocatalysts were conducted in triplicates. Blank experiments without photocatalyst were also conducted separately to investigate various possible mass losses due to BPA photolysis and adsorption to photoreactor or filter.

2.6. Analysis of solution sample

The concentrations of BPA were measured using Perkin Elmer Series200 HPLC, with acetonitrile and water as the mobile phase at 80/20 volume ratio and a flow rate of 1 mL/min. Finally, after 6 h of irradiation, the total organic carbon (TOC) remained in the solution was determined using a Shimadzu ASI-V TOC Analyzer. A selective numbers of aqueous samples, namely, the solutions at 2 h and 6 h

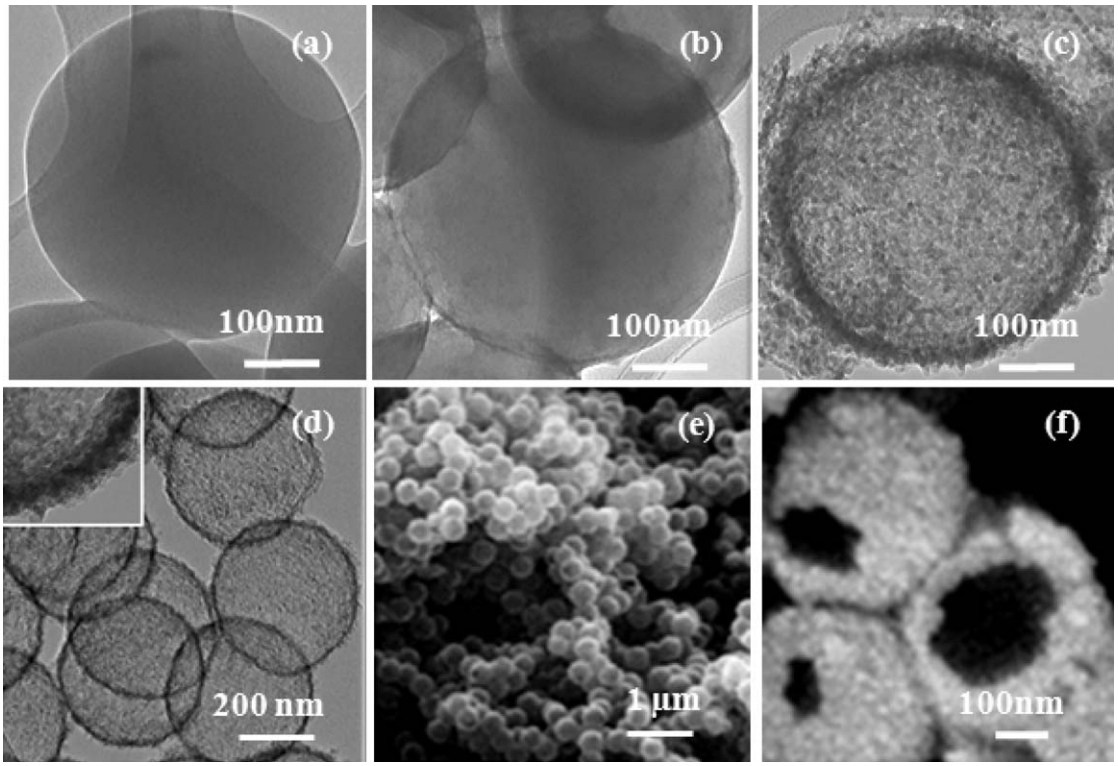

Fig. 3. Transmission electron microscope (TEM) images of (a) polystyrene sphere, (b) titania sol coated PS sphere, (c) N-doped TiO_2 hollow sphere (NhT) after calcination, (d) a cluster of NhT spheres, scanning electron micrographs (SEM) of (e) monodispersed NhT spheres, and (f) typical broken spheres. The inset in (d) displays the wall thickness of the spheres.

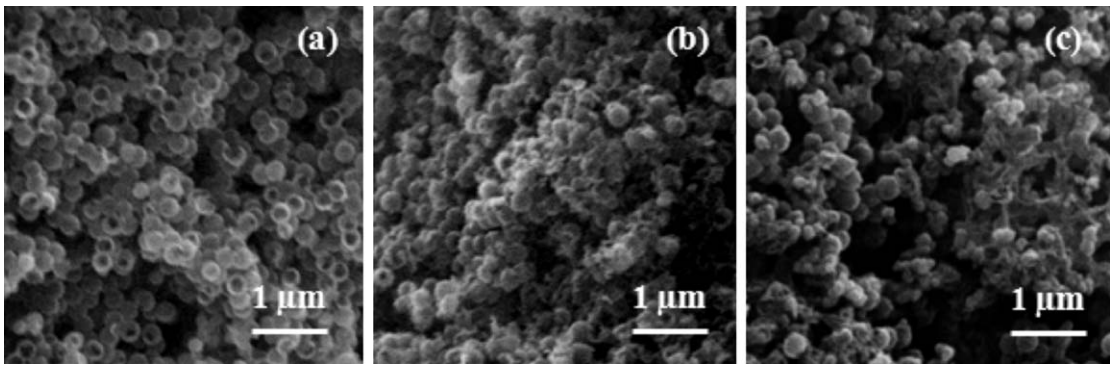

Fig. 4. SEM images of N-doped TiO_2 hollow spheres calcined at (a) 500 °C, (b) 600 °C, and (c) 700 °C.

reactions under blue LED irradiation as well as the blank solution and the solutions after adsorption in dark, were also filtered and analyzed for the intermediate species formed during photocatalytic degradation of BPA or any impurities in the BPA stock solution. The samples were analyzed using Agilent 6890/5975 gas chromatography–mass spectrometry (GC/MS) with a DB-5MS (30 m × 0.25 mm × 0.25 μm) silica capillary column and Agilent 1200SL-6460 Rapid Resolution LC/MS/MS with Agilent Zorbax Eclipse Plus C18 column (100 mm × 2.1 mm × 1.8 μm). For analyses with GC/MS, liquid–liquid extraction (LLE) using methylene chloride or ethyl acetate was performed on solution aliquots sampled from the photoreactor. An injection volume of 1 μL was injected into the GC/MS instrument in splitless mode. The carrier gas was helium introduced at constant flow rate of 1.0 mL/min. The temperature of the column was programmed from 40 °C (held for 4 min) to 270 °C at 10 °C/min and held for 16 min at 270 °C. The analysis was performed in the electron-impact (EI) ionization mode at 70 eV. Indirect quantification of the detected compounds was obtained based on the peak area ratios against acenaphthene-d10 (internal standard). For analyses with LC/MS/MS, qualitative finding was to be obtained. The mobile phase A was 5 mM ammonium acetate in HPLC water while the mobile phase B was methanol, and the mobile phase was introduced at a flow rate of 0.3 mL/min. The sample injection volume was 1 μL. The instrument was operated in the negative ionization mode.

3. Results and discussion

3.1. Morphology

Monodispersed N-doped TiO_2 hollow spheres (NhT) were successfully synthesized by uniform coating of PS templates using sol–gel precursor solution followed by calcination at 500 °C to crystallize titania and simultaneously remove PS spheres leaving behind a hollow core. The synthesized PS spheres were with an average diameter of ca. 400 nm (Fig. 3a), and its diameter increased to ca. 430 nm after coating with titania sol (Fig. 3b). The average diameter of synthesized NhT spheres (Fig. 3c) was ca. 360 nm, indicating 15% shrinkage in diameter resulting from calcination at 500 °C, which was commonly observed in hollow spheres prepared through templating and calcination [22,25]. The hollow spherical morphology of NhT is shown in Fig. 3d, while its inset shows the wall thickness of ca. 20 nm made up of the aggregated TiO_2 crystallites with the sizes of 10–20 nm. The NhT uniformity in size can be seen in Fig. 3e. Some broken NhT spheres were also observed (Fig. 3f). Indeed, increasing the calcination temperatures to 600 °C and 700 °C was found to result in the disintegration of spherical morphology (Fig. 4). It was observed that coated spheres calcined at 500 °C appeared pale yellow in color whereas those calcined at 600 °C and 700 °C appeared as light yellow and white samples, respectively. This may be attributed to the reduction in nitrogen doping level into titania at higher calcination temperatures [26,27].

3.2. Photocatalysts surface area and pore size determination

The Brunauer–Emmett–Teller (BET) surface areas and porosities of all samples are shown in Table 1. PT possessed a specific surface area of only ca. 36 m^2/g while hollow titania (hT) and NhT exhibited higher surface area of ca. 90 m^2/g and 80 m^2/g, respectively. Compared to 0.08 cm^3/g of pore volume for PT, hT and NhT had greater pore volumes of ca. 0.18 cm^3/g and 0.16 cm^3/g, respectively which are associated with mesopores within their sphere walls. The significantly larger BET surface area and mesopore volume indicate that introduction of hollow morphology (in NhT and hT) yielded more porous structure in the sphere wall.

3.3. Crystal structure analysis of photocatalysts

Anatase phase of titania is photocatalytically more active than other polymorphs (rutile, brookite, TiO_2-B) [28]. Fig. 5 shows the powder X-ray diffraction pattern of the various photocatalysts synthesized in this work. Only anatase phase of titania was detected in all the samples, because the calcination temperature employed (500 °C) was less than the transition temperature from anatase to rutile that occurs at temperatures higher than ca. 600 °C [28]. Rietveld qualitative phase analyses (using TOPAS software) revealed crystallite sizes of ca. 15–18 nm for all photocatalysts

Table 1
BET surface areas, pore volumes, pore diameters, crystallite sizes and atomic contents of photocatalysts.

Sample	Surface area (m^2/g)	Pore volume[a] (cm^3/g)	Pore diameter[b] (nm)	Crystallite size (nm)	Relative content (%)			
					Ti2p	N1s	O1s	C1s
PT	36.1 ± 0.2	0.078	6.6	18.2 ± 0.6	6.61	BDL	42.15	51.23
hT	90.2 ± 1.5	0.176	3.6	15.7 ± 0.7	7.84	BDL	46.69	45.47
NhT	80.1 ± 1.2	0.163	3.8	16.1 ± 0.7	3.32	0.68	41.60	54.40

BDL, below detection limit of the equipment.
[a] Pore volume calculated from BJH desorption curve.
[b] Average pore diameter calculated from BJH desorption curve, and indicating average pore size between primary particles.

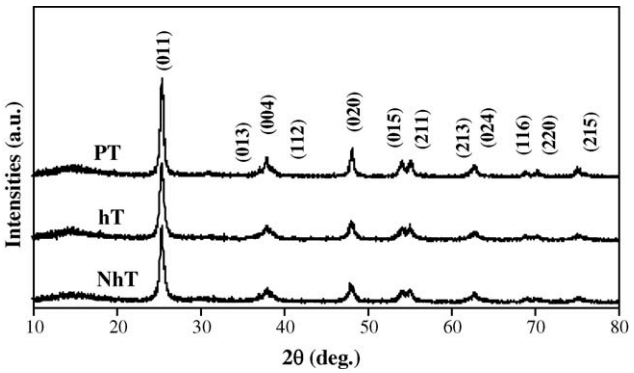

Fig. 5. X-ray diffraction patterns of photocatalysts.

(Table 1) which is also evidenced by their TEM images (e.g., inset of Fig. 3d) that show individual crystalline domains of ca. 10–20 nm.

3.4. XPS analysis of photocatalysts

The atomic percentages of elements (Ti, N, O, C) present in all samples deduced from wide survey XPS are included in Table 1. The NhT sample is found to contain 0.68% N whilst nitrogen was not detected in both PT and hT. The high-resolution N1s spectra with binding energies of the three samples are shown in Fig. 6. For NhT, the N1s peaks are observed at 400.5 eV and 404.8 eV (Fig. 6a). The absence of N1s peak at 396–397 eV indicates that no nitridic nitrogen in N–Ti–N linkages is formed [29]. Subsequently, we assign the peak at 400.5 eV oxidized nitrogen in O–Ti–N or Ti–O–N linkages [27,30,31]. When nitrogen atom substitutes oxygen in O–Ti–O linkages, the electron density around nitrogen atom is reduced. Since oxygen is more electronegative than nitrogen, the binding energy of nitrogen in O–Ti–N or Ti–O–N linkages should be higher than that in N–Ti–N linkages. The other N1s peak with binding energy of 404.8 eV is attributed to nitrite ions [32]. It is worth mentioning that assignment of N1s XPS peaks in N-doped titania is ambiguous. Contrary to the general notion that attributed visible light photocatalytic ability of titania to an N1s peak of 396–397 eV [17,29,33], some indicated that N1s peaks with relatively higher binding energies (399–408 eV) should also been considered carefully [32,34,35]. For both PT (Fig. 6c) and hT (Fig. 6e) samples, no N1s peak is observed.

High-resolution spectra of Ti2p of NhT supported the findings of nitrogen incorporation in O–Ti–N linkages. As shown in Fig. 6b, other than typical TiO_2 peaks of 458.7 eV ($Ti2p_{3/2}$) and 464.6 eV

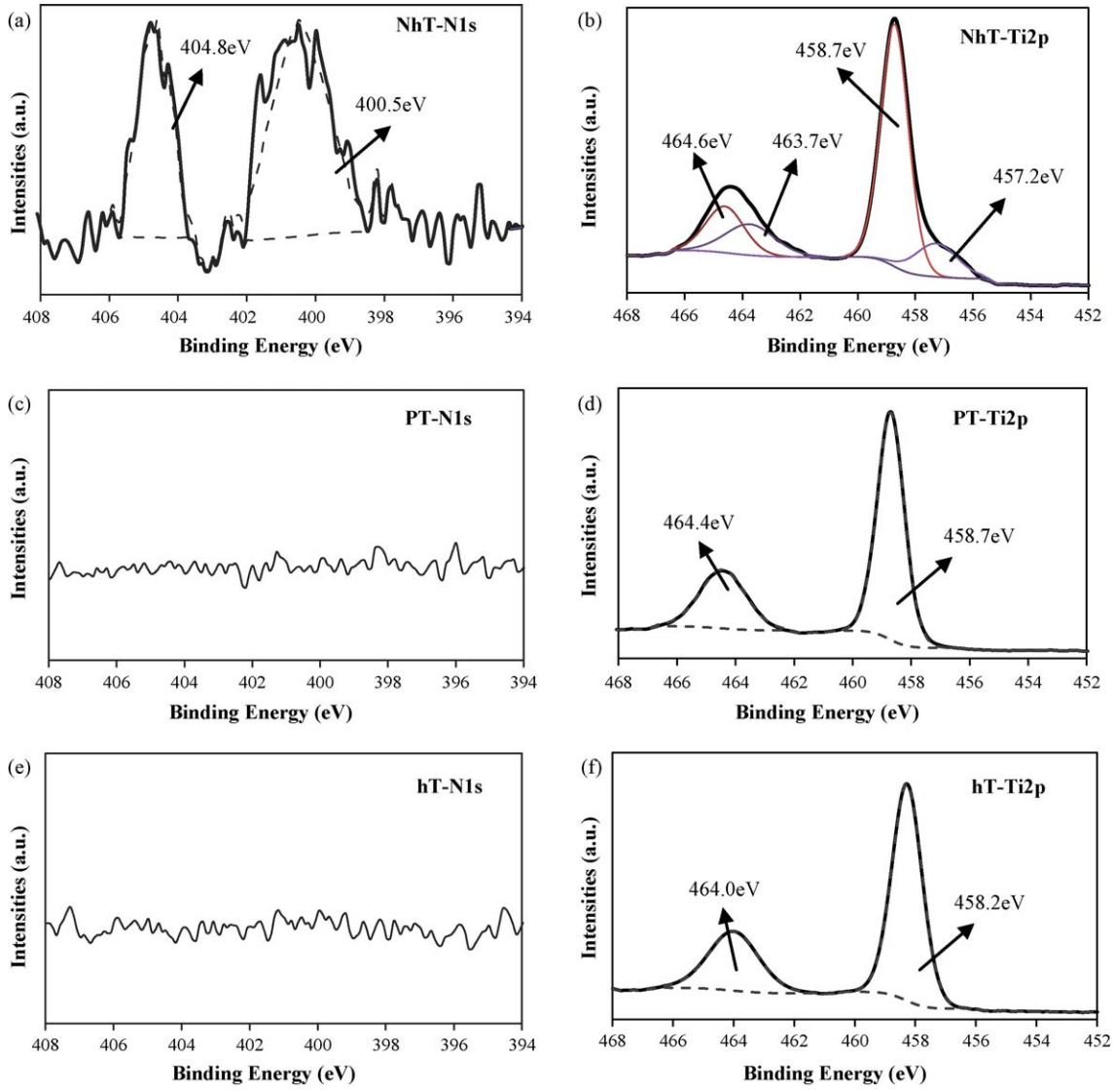

Fig. 6. Comparison of XPS spectra of N1s peaks and Ti2p peaks of various photocatalysts.

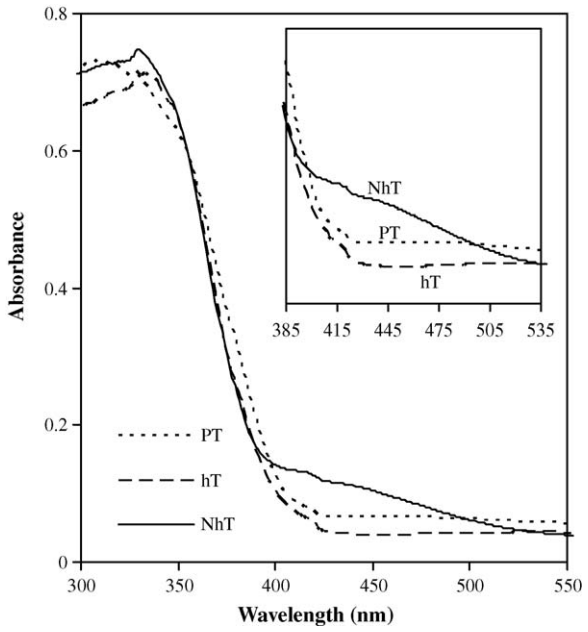

Fig. 7. UV–visible absorption spectra of photocatalysts.

($Ti2p_{1/2}$), another pair of Ti2p peaks is observed at 457.2 eV ($Ti2p_{3/2}$) and 463.7 eV ($Ti2p_{1/2}$). The emergence of Ti2p peaks of lower binding energies may results from the presence of O–Ti–N or Ti–N–O linkages. Since oxygen is more electronegative than nitrogen, nitrogen substitution causes an increase of electron density around Ti atom [31] resulting in the decrease of binding energy of Ti2p peaks. Deconvolutions of Ti2p peaks of PT (Fig. 6d) and hT (Fig. 6f) samples revealed only typical $Ti2p_{1/2}$ peak at 464.4 eV and 464.0 eV, and $Ti2p_{3/2}$ peak at 458.7 eV and 458.2 eV, respectively found in titania.

3.5. UV–vis diffuse reflectance spectroscopy

The UV–vis absorption spectra of the samples are shown in Fig. 7. The absorption edge of PT is ca. 410 nm (E_g = 3.02e V), while that of hT and NhT are approximately 400 nm (E_g = 3.10 eV). The shift in the absorption edge of samples with hollow structures towards shorter wavelengths might be due to quantum size effects [21,36]. In addition, NhT sample exhibits a shoulder absorbance in the visible light spectrum, with the absorption threshold for this second absorption edge at ca. 550 nm (E_g = 2.26 eV). This is an indication of nitrogen doping into titania [17,34,37].

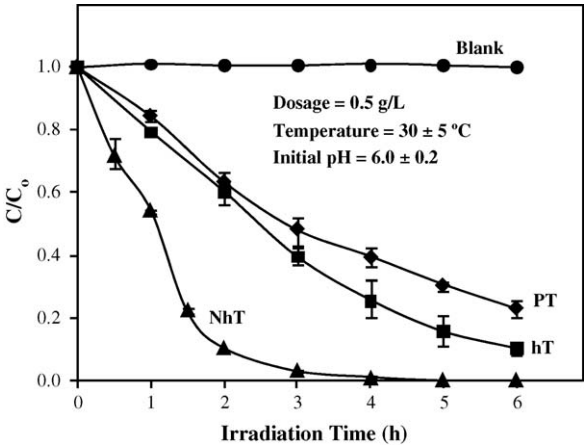

Fig. 8. Photocatalytic degradation of BPA with different photocatalysts under irradiation of blue LED.

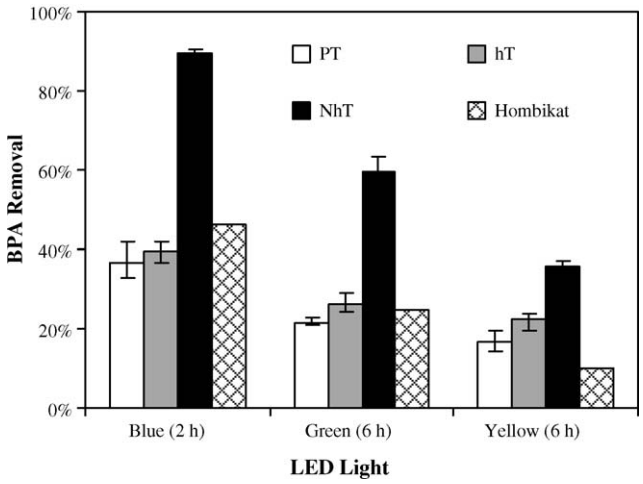

Fig. 9. Comparison of BPA removal efficiencies with various photocatalysts and LEDs emitting different light colors.

3.6. Photocatalytic degradation

3.6.1. Photocatalytic degradation kinetics

Analysis of sample aliquots taken at the end of 1 h in dark (before commencement of the photocatalytic reaction experiment) showed that the initial BPA concentrations in photoreactors containing different photocatalysts remained rather constant (ca. 5.0 mg/L). After light on, BPA concentration in the photoreactor containing photocatalysts started to decrease. Fig. 8 shows rapid decrease in the BPA concentration in the photoreactor containing NhT under irradiation of blue light. Control experiments in the absence of photocatalyst showed negligible BPA photolysis throughout 6 h of LED irradiation (the slight increases in BPA concentration could be due to water evaporation). After 6 h of irradiation, all photocatalysts displayed remarkable degradation of BPA. It is apparent that nitrogen doping of NhT significantly accelerated BPA degradation. Both photocatalysts with hollow morphologies (NhT and hT) were more photoactive than PT, indicating the advantage of having a relatively more porous structure in photocatalysts. Even though doping with nitrogen slightly reduced the effective surface area and pore volume of NhT compared to those of hT, the intrinsic benefit of nitrogen doping is evident. Indeed, 90% of BPA was removed within 2 h with NhT as compared to ca. 40% with hT and 35% with PT photocatalysts under the blue LED irradiation.

Fig. 9 shows that NhT was significantly superior to PT, hT and Hombikat UV100 for BPA degradation under different colors of LED irradiations. It is obvious that when the LEDs used were changed from blue (λ = 465 nm) to green (λ = 523 nm) and yellow (λ = 589 nm), decreasing BPA degradation efficiencies occurred with the photocatalysts. Theoretically, both PT and hT, with their absorption edge at 400–410 nm, respectively, should not degrade BPA under visible light. However, both appeared to be capable of degrading a small fraction of BPA even under yellow light. There could be trace near-UV emission from the LEDs. Using a Digital Power Meter SP 1065 (Janco Impex), the measured UV intensities in the irradiations from the three types of LEDs were $<70\ \mu W/cm^2$. Further UV measurement using Accumax XRP-3000 radiometer did not detect UV emission at 365 nm. Indeed, the UV component emitted from the three types of LEDs was also too weak to induce photolysis of BPA in the bulk solution, which was also revealed from the result of our blank experiments. Comparing hT and PT, under green and yellow light irradiations, the slight increment in BPA removal with hT over that exhibited by PT could be attributed

Table 2
Pseudo-first-order kinetics for photocatalytic degradation of BPA using various photocatalysts at various reaction conditions.

Sample	Blue LED		Green LED		Yellow LED	
	k' (h^{-1})	R^2	k' (h^{-1})	R^2	k' (h^{-1})	R^2
PT (pH 6.0)	0.238	0.996	0.034	0.931	0.034	0.932
hT (pH 6.0)	0.353	0.977	0.048	0.981	0.040	0.978
NhT (pH 6.0)	1.131[a]	0.989	0.148	0.976	0.076	0.969
NhT (pH 3)	0.507[a]	0.971				
NhT (pH 10)	1.342[a]	0.971				

[a] Within the initial 3 h of reaction.

to the significantly greater surface area of hT that induced more BPA photocatalytic degradation on photocatalyst surface.

The following Langmuir–Hinshelwood model has been widely applied to delineate the kinetics of heterogeneous photocatalytic degradation of pollutants in aqueous phase [38]:

$$r_o = -\left(\frac{d[\mathrm{BPA}]}{dt}\right) = \frac{kK[\mathrm{BPA}]}{1 + K[\mathrm{BPA}]} \quad (1)$$

where r is the rate of BPA mineralization, [BPA] is the concentration of BPA, t is the reaction time, k is the intrinsic reaction rate constant, and K is the Langmuir adsorption equilibrium constant. The model takes into accounts the surface processes which are mediated by photocatalyst and involved •OH produced on the photocatalyst surface. At a dilute BPA concentration (e.g., $[\mathrm{BPA}]_o \sim 0.02$ mM in our experiments), pseudo-first-order kinetics can be assumed since minimum BPA adsorption was also observed in this study (i.e., $K[\mathrm{BPA}] \ll 1$) [38]. Thus:

$$r_o = -\left(\frac{d[\mathrm{BPA}]}{dt}\right) = kK[\mathrm{BPA}] \quad (2)$$

$$\ln\left(\frac{[\mathrm{BPA}]}{[\mathrm{BPA}]_o}\right) = -kKt = -k't \quad (3)$$

where k' is the pseudo-first-order rate constant. The calculated k' values for experiments with the synthesized photocatalysts are shown in Table 2. Under the LED blue and green light irradiations, the reaction rate with NhT is three times that of hT, indicating the evidence of enhanced photoactivity of the NhT under visible light due to nitrogen doping. The rates decreased remarkably as the wavelengths of the visible light irradiation increased (by comparing blue, green and yellow lights). Nevertheless, it is evident that the NhT was still able to be photoexcited by the yellow light.

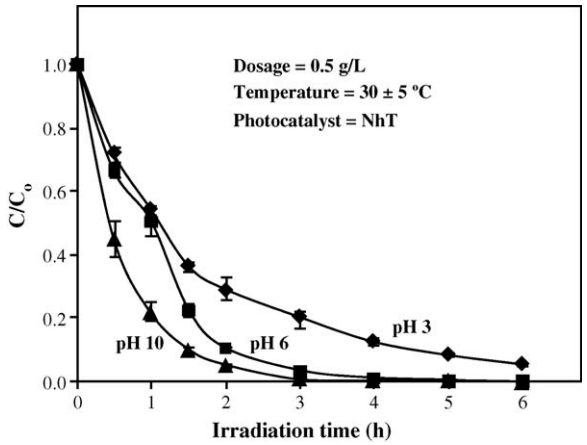

Fig. 10. Effect of pH on photocatalytic degradation of BPA with NhT under irradiation of blue LED.

For an amphoteric material such as TiO_2 [39], the change in the concentrations of H^+ and OH^-can affect its net surface charges. Fig. 10 shows that BPA photocatalytic degradation rate with NhT increased as the reaction medium was changed from acidic to alkaline condition. The points of zero charge (PZC) of NhT as measured with the Malvern nano-zs zetasizer was at pH 5.36, which is slightly lower than that of anatase TiO_2 [40]. Thus, at pH 6 and pH 10 the NhT carried a net negative charge. Meanwhile, BPA primarily exists as BPA^- or BPA^{2-} ion species at pH 10, which is between p*K*a1 (pH 9.6) and p*K*a2 (pH 10.2) of BPA [41]. Apparently, the increasing BPA degradation rate with pH could be attributed to the increased concentration of hydroxyl radicals (•OH) produced. This indicates that the BPA photocatalytic degradation under visible light with the hollow sphere photocatalyst was predominantly due to •OH attack. Similar finding for BPA photocatalytic degradation under UV with TiO_2 anatase powder has also been reported [13].

3.6.2. Mineralization of BPA and intermediates

Fig. 11 shows the extent of TOC removal along with BPA degradation which indicates the degree of BPA mineralization after 6 h irradiation under blue LEDs. Concomitant with 99% BPA removal using NhT, approximately 66% of organic carbon had been completely mineralized (Fig. 11a). These efficiencies were higher than those exhibited by Hombikat UV100 which has at least three

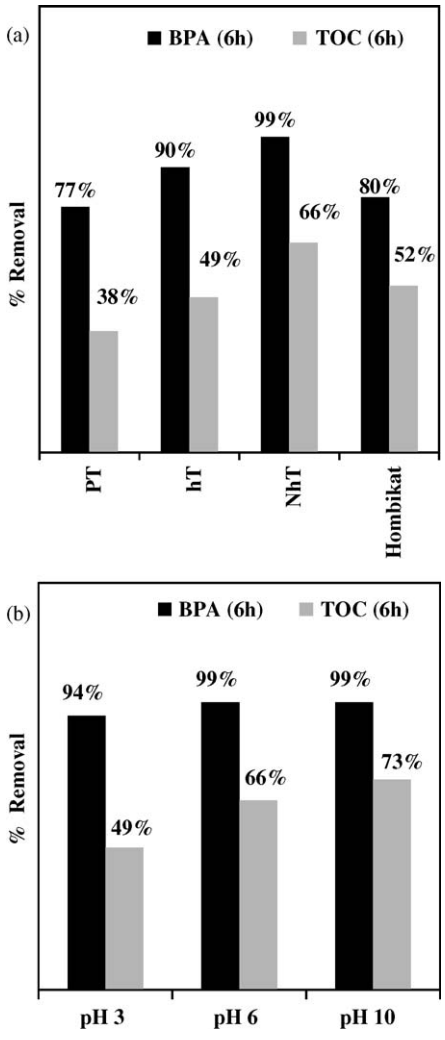

Fig. 11. Photocatalytic mineralization of BPA under LED blue light. (a) Comparison of performance by various photocatalysts at pH 6.0 and (b) effect of pH with NhT as photocatalyst.

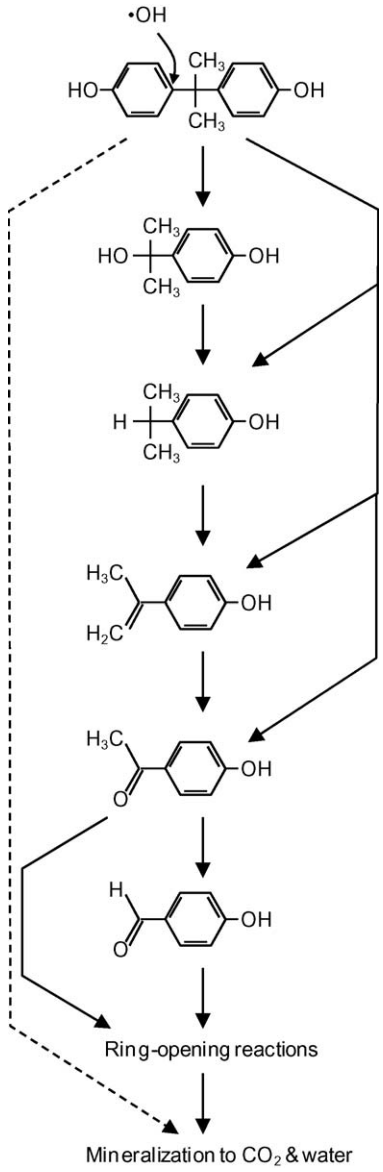

Fig. 12. Possible photocatalytic degradation pathways of BPA with nitrogen-doped TiO_2 hollow sphere irradiated by vis-LED.

times higher BET surface area, attributable to the hollow spherical morphology and the nitrogen doping of NhT. A higher degree of mineralization was achieved at higher pH (Fig. 11b). The residual TOC remained in the photoreactor after 6 h of irradiation indicated formation of more persistent intermediates that might require longer irradiation to degrade.

For the solutions containing NhT irradiated by blue LED light, analysis with LC/MS/MS consistently revealed the formations of several aromatic intermediates which have been reported previously in the studies of BPA photocatalytic oxidation with UV-irradiated TiO_2 (UV/TiO_2). These compounds include 4-isopropanolphenol (m/z = 151), 4-isopropylphenol (m/z = 135), 4-isopropenylphenol (m/z = 133), and 4-hydroxyacetophenone (m/z = 135). 4-hydroxybenzaldehyde (m/z = 121) was also detected but its characteristic peaks were rather low compared to those of other compounds. It was observed that when the reaction continued from 2 h to 6 h, the concentration of 4-hydroxyacetophenone increased in tandem with the decrease of 4-isopropanolphenol and 4-isopropenylphenol. 4-Hydroxyacetophenone appeared to be the most prominent aromatic intermediate in the photoreactors containing NhT after 6 h of irradiation with blue LED light. Quantitative analysis with GC/MS showed that the concentration ratio of 4-isopropenylphenol:BPA increased from 0.38 at 2 h of reaction to 1.25 at 6 h of reaction, due to decreased BPA concentration. 4-Isopropenylphenol was also detected in the reactor containing hT, but its concentrations ranged from 12% to 30% of those detected in the reactors with NhT.

The photocatalytic degradation pathways for BPA based on UV/TiO_2 system have been proposed previously by researchers [7,11,12,16], though discrepancies remain. Based on the relative abundances of the five aromatic intermediates and their changes with reaction time as revealed in this study, the possible pathways for BPA degradation under visible light may follow the scheme as proposed in Fig. 12. Generally, BPA photocatalytic degradation was believed to be initiated through attacks by •OH at the electron-rich C3 in the phenyl group of BPA [7,16]. This is followed by the cleavage of the two phenyl groups into formations of 4-isopropanolphenol [7,12,15,16], 4-isopropylphenol [7,16], 4-isopropenylphenol [11] or 4-hydroxyacetophenone [7], either sequentially or directly through formations of transient intermediates or radicals (e.g., $^{\bullet}C(CH_3)_2C_6H_4OH$ and $^{\bullet}H$ [16]). Immediate ring cleavage by •OH attack of BPA to form 3-hydroxy-1,3,5-hexadiene has been also proposed previously for UV/TiO_2 [7,12] and it could lead directly to the formation of aliphatic acids and eventual mineralization.

4. Practical significance and conclusion

The development of hollow sphere TiO_2 promises several advantages compared to the powder TiO_2. Its high surface area, high porosity and low bulk density will enhance photonic efficiency and dispersivity in photoreactor. To harness the abundant solar energy for photo-excitation of the hollow sphere TiO_2, nitrogen doping of the TiO_2 hollow spheres can be successfully prepared through polystyrene templating method, treatment with ammonia solution and careful selection of calcination temperature. There appears to have a narrow range of specific calcination temperature, outside which will result in unsuccessful preparation. The NhT photocatalyst synthesized in this study exhibited an action spectrum extending to yellow light, with respect to photocatalytic degradation of BPA. This suggests possible solar incorporation for BPA destruction in photocatalytic reactor during day time, and use of artificial lights during dark. The use of LED flexible strip as alternative light source allows adaptable photoreactor configurations that can be incorporated into integrated treatment system such as membrane photoreactor for effective separation and recovery of photocatalyst from the treated water.

Acknowledgement

National Research Foundation (NRF), Singapore, is acknowledged for the financial support through the project EWI RFP 0802-11 for development of new-generation photocatalysts to be used in water purification.

References

[1] J.-H. Kang, D. Aasi, Y. Katayama, Critical Reviews in Toxicology 37 (2007) 607–625.
[2] A.V. Krishnan, P. Stathis, S.F. Permuth, L. Tokes, D. Feldman, Endocrinology 132 (1993) 2279–2286.
[3] C.A. Staples, P.B. Dorn, G.M. Klecka, S.T. O'Block, L.R. Harris, Chemosphere 36 (1998) 2149–2173.
[4] J. Jackson, R. Sutton, Science of the Total Environment 405 (2008) 153–160.
[5] D.W. Kolpin, E.T. Furlong, M.T. Meyer, E.M. Thurman, S.D. Zaugg, L.B. Barber, H.T. Buxton, Environmental Science and Technology 36 (2002) 1202–1211.
[6] P.E. Stackelberg, E.T. Furlong, M.T. Meyer, S.D. Zaugg, A.K. Henderson, D.B. Reissman, Science of the Total Environment 329 (2004) 99–113.

[7] S. Horikoshi, T. Miura, M. Kajitani, N. Horikoshi, N. Serpone, Applied Catalysis B: Environmental 84 (2008) 797–802.
[8] F.J. Rivas, E. Ángel, A. Benito, J.B. Fernando, Journal of Chemical Technology and Biotechnology 84 (2009) 589–594.
[9] W.-T. Tsai, M.-K. Lee, T.-Y. Su, Y.-M. Chang, Journal of Hazardous Materials 168 (2009) 269–275.
[10] Y. Ohko, I. Ando, C. Niwa, T. Tatsuma, T. Yamamura, T. Nakashima, Y. Kubota, A. Fujishima, Environmental Science and Technology 35 (2001) 2365–2368.
[11] S. Fukahori, H. Ichiura, T. Kitaoka, H. Tanaka, Applied Catalysis B: Environmental 46 (2003) 453–462.
[12] K. Nomiyama, T. Tanizaki, T. Koga, K. Arizono, R. Shinohara, Archives of Environmental Contamination and Toxicology 52 (2007) 8–15.
[13] S. Kaneco, M.A. Rahman, T. Suzuki, H. Katsumata, K. Ohta, Journal of Photochemistry and Photobiology A: Chemistry 163 (2004) 419–424.
[14] S.-M. Chang, P.-H. Lo, C.-T. Chang, Applied Catalysis B: Environmental 91 (2009) 619–627.
[15] H.R. Kim, Y. Eom, T.G. Lee, Y.-G. Shul, Materials Chemistry and Physics 108 (2008) 154–159.
[16] N. Watanabe, S. Horikoshi, H. Kawabe, Y. Sugie, J. Zhao, H. Hidaka, Chemosphere 52 (2003) 851–859.
[17] R. Asahi, T. Morikawa, T. Ohwaki, K. Aoki, Y. Taga, Science 293 (2001) 269–271.
[18] S.-J. Ding, C.-L. Zhang, M. Yang, X.-Z. Qu, Y.-F. Lu, Z.-Z. Yang, Polymer 47 (2006) 8360–8366.
[19] I.A. Kartsonakis, P. Liatsi, I. Danilidis, D. Bouzarelou, G. Kordas, Journal of Physics and Chemistry of Solids 69 (2008) 214–221.
[20] G.K. Li, Z.C. Zhang, Materials Letters 58 (2004) 2768–2771.
[21] C. Song, W. Yu, B. Zhao, H. Zhang, C. Tang, K. Sun, X. Wu, L. Dong, Y. Chen, Catalysis Communications 10 (2009) 650–654.
[22] A. Syoufian, Y. Inoue, M. Yada, K. Nakashima, Materials Letters 61 (2007) 1572–1575.
[23] D. Wang, C. Song, Y. Lin, Z. Hu, Materials Letters 60 (2006) 77–80.
[24] T.E. Doll, F.H. Frimmel, Water Research 38 (2004) 955–964.
[25] M. Agrawal, A. Pich, N. Zafeiropoulos, M. Stamm, Colloid and Polymer Science 286 (2008) 593–601.
[26] S. Sato, R. Nakamura, S. Abe, Applied Catalysis A: General 284 (2005) 131–137.
[27] X. Wang, J.C. Yu, Y. Chen, L. Wu, X. Fu, Environmental Science and Technology 40 (2006) 2369–2374.
[28] O. Carp, C.L. Huisman, A. Reller, Progress in Solid State Chemistry 32 (2004) 33–177.
[29] N.C. Saha, H.G. Tompkins, Journal of Applied Physics 72 (1992) 3072.
[30] T.C. Jagadale, S.P. Takale, R.S. Sonawane, H.M. Joshi, S.I. Patil, B.B. Kale, S.B. Ogale, The Journal of Physical Chemistry C 112 (2008) 14595–14602.
[31] G.-S. Shao, X.-J. Zhang, Z.-Y. Yuan, Applied Catalysis B: Environmental 82 (2008) 208–218.
[32] S. Sakthivel, M. Janczarek, H. Kisch, The Journal of Physical Chemistry B 108 (2004) 19384–19387.
[33] H. Irie, Y. Watanabe, K. Hashimoto, The Journal of Physical Chemistry B 107 (2003) 5483–5486.
[34] Y. Cong, J. Zhang, F. Chen, M. Anpo, The Journal of Physical Chemistry C 111 (2007) 6976–6982.
[35] J.L. Gole, J.D. Stout, C. Burda, Y. Lou, X. Chen, The Journal of Physical Chemistry B 108 (2004) 1230–1240.
[36] M. Anpo, T. Shima, S. Kodama, Y. Kubokawa, The Journal of Physical Chemistry 91 (1987) 4305–4310.
[37] X. Chen, C. Burda, Journal of the American Chemical Society 130 (2008) 5018–5019.
[38] J.M. Herrmann, Topics in Catalysis 34 (2005) 49–65.
[39] A. Fahmi, C. Minot, Surface Science 304 (1994) 343–359.
[40] T. Sugimoto, X. Zhou, Journal of Colloids and Interface Science 252 (2002) 347–353.
[41] P.G. Kosky, J.M. Silva, E.A. Guggenheim, Industrial and Engineering Chemistry Research 30 (2002) 462–467.